Macromolecules

Article

pubs.acs.org/Macromolecules

Rheokinetics of Ring-Opening Metathesis Polymerization of Bio-Based Castor Oil Thermoset

Samy A. Madbouly,[†,⊥] Ying Xia,[†] and Michael R. Kessler*[,†,‡,§]

[†]Department of Materials Science and Engineering, Iowa State University, Ames, Iowa 50011, United States

[‡]Department of Mechanical Engineering, Iowa State University, Ames, Iowa 50011, United States

[§]Ames Laboratory, US Department of Energy, Ames, Iowa 50011, United States

[⊥]Faculty of Science, Department of Chemistry, Cairo University, Orman-Giza 12613, Egypt

ABSTRACT: Ring-opening metathesis polymerization (ROMP) of norbornenyl-functionalized castor oil has been evaluated using small-amplitude oscillatory shear flow experiments as a function of angular frequency, temperature, and curing time. At the onset temperature of the curing process, an abrupt increase in dynamic shear moduli, G' and G'', and complex shear viscosity, η^*, was observed during the dynamic temperature ramps (2 °C/min heating rate) of the sample over a wide range of angular frequencies. A dramatic increase in zero-shear viscosity, η_0, was also observed at the gelation temperature, T_{gel}. The value of T_{gel} obtained from the abrupt increase in η_0 was found to be in good agreement with the value evaluated from the crossover point of G' and G''. The real time curing kinetics was investigated under isothermal conditions over a wide range of angular frequencies at different constant curing temperatures (40, 45, 50, and 55 °C). The isothermal gelation kinetics was found to be strongly curing temperature dependent; i.e., the higher the curing temperature, the faster the gelation process. Both G' and G'' showed a power law relationship with angular frequency at the gel point, with critical power law exponents at the gel point in good agreement with the value predicted using percolation theory. Furthermore, η_0 and the equilibrium storage modulus, G_{eq}, were found to be well described by power law scaling functions with the relative distance from the gel point. The molecular dynamics and thermal stability of the fully cured sample were also investigated by dynamic mechanical analysis and thermogravimetry, respectively.

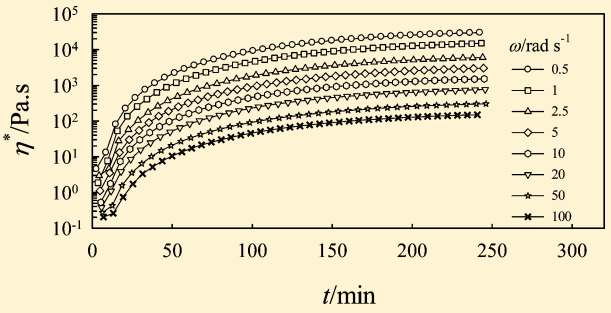

INTRODUCTION

Polymers are as ubiquitous as they are essential for a plethora of consumer and high technology applications. Currently, most industrial polymers and plastics are produced from non-renewable, petrochemical resources. However, concerns regarding petroleum depletion and the growing cost of oil, as well as the environmental impact of such materials, have led to an increased interest in alternative, sustainable, environmentally friendly materials based on renewable resources. Bio-based polymers have a number of outstanding desirable characteristics, such as abundant availability from renewable agricultural resources, low cost, biodegradability (most of them), high thermal stability, and noncytotoxicity (inflammatory inert). Biorenewable polymers from vegetable oils are excellent alternatives to petroleum-based resins for both environmental and economic reasons. With the exception of castor oil, vegetable oils do not naturally contain hydroxyl groups (often necessary for chemical modification and/or polymerization), but rather hydroxyl groups can be introduced through appropriate chemical modifications on the carbon−carbon double bonds and the ester functionality present in triglycerides. Castor oil's unique structure, with ∼90% of the fatty acid chains bearing a hydroxyl group, makes it a very useful vegetable oil in industry.[1] A wide variety of polymers, especially castor oil-based polyurethanes, were prepared by taking advantage of these naturally occurring hydroxyl groups.[2]

Olefin metathesis, which is a relatively new polymerization method,[3] has been employed to prepare vegetable oil-based polymers. For example, recently, acyclic diene (triene) metathesis polymerization (ADMET/ATMET) was used to prepare plant oil-based polymers.[4] Novel biorenewable materials were prepared by ring-opening metathesis polymerization (ROMP) as well. For example, two kinds of ROMP-based systems, norbornenyl anhydride-functionalized castor oil (BCO)/cyclooctene (CO)[5] and Dilulin (a norbornenyl-functionalized linseed oil)[6]/dicyclopentadiene (DCPD)),[7] were previously developed in our group. Both systems afford green thermosets and provide a promising new route to bioplastics from biorenewable resources. However, some improvements need to be made to obtain well-controlled and precise ROMP for bioplastics production.

Fundamental investigations of the kinetics of ROMP reactions are a promising area for research to obtain better understanding of the cure behavior and of the mechanism of

Received: July 13, 2012
Revised: August 18, 2012
Published: September 24, 2012

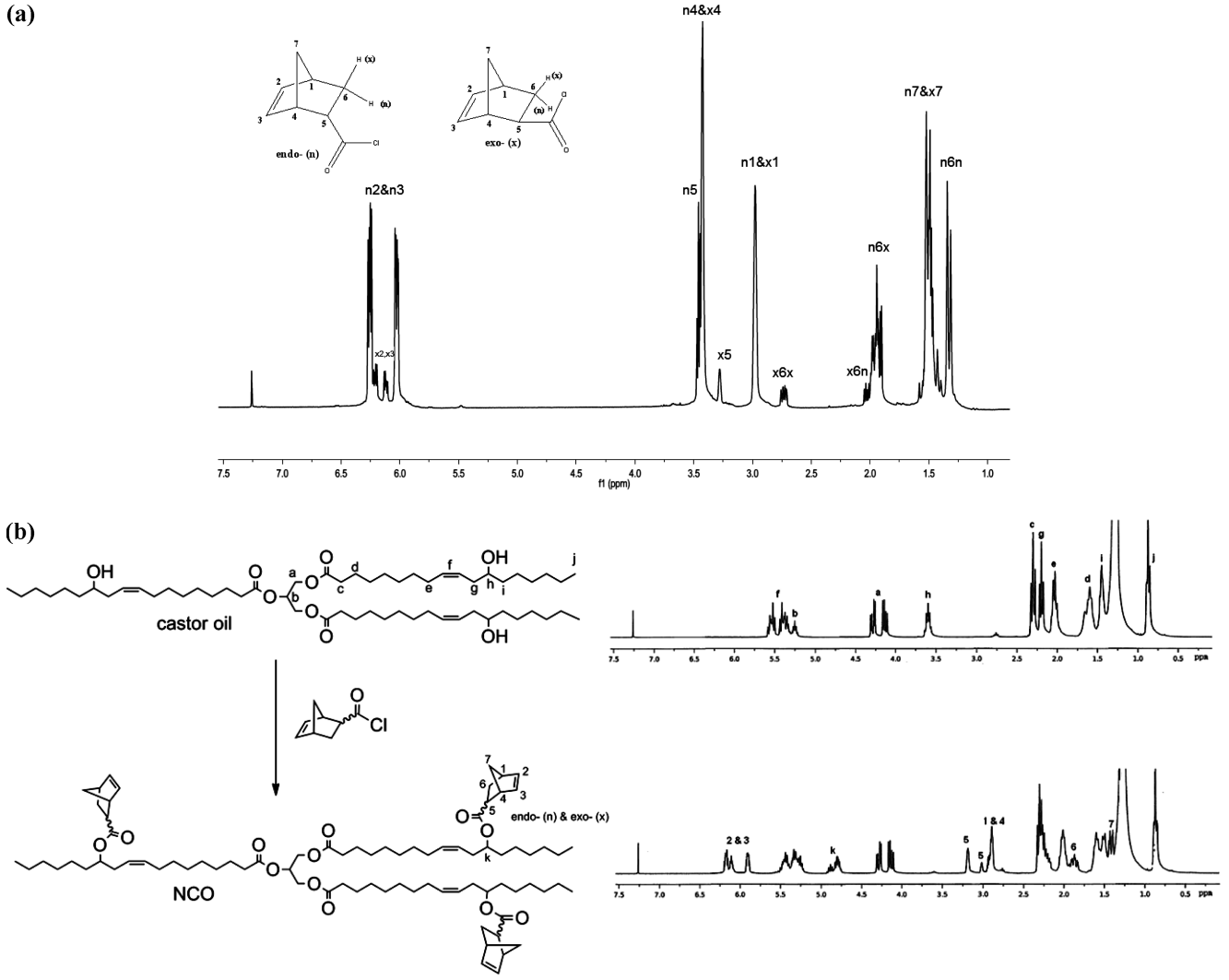

Figure 1. (a) Peak assignments of the ^{1}H NMR for the pure BHCC sample. (b) Chemical structures of castor oil and norbornenyl-functionalized castor oil (NCO) with their ^{1}H NMR spectra.

macroscopic gelation (formation of three-dimensional thermoset structure). It may also prove useful for controlling the production process and final performance of the systems. Although in the past decades many studies focused on cross-linked thermosetting resins, the network formation mechanism and the fine structure of cross-linked resins are still controversial topics because of the complexity of the reactions involved and the insolubility of the products.[8] The kinetics of cross-linking reactions has been investigated by a wide range of experimental techniques, such as ^{13}C NMR (nuclear magnetic resonance),[9−12] SEC (size exclusion chromatography),[13,14] DSC (differential scanning calorimetry),[15−18] and FTIR[19−21] (Fourier transform infrared spectroscopy). Mechanical characterizations were also performed by measuring Young's modulus or swelling ratio. However, measurements obtained from Young's modulus or swelling ratio experiments do not reveal the kinetics of curing and are therefore not useful in determining the optimal cross-linking reaction with desired properties. In most studies reported in the literature, the samples were cured isothermally for different time intervals before being analyzed.

Dynamic rheology is one of the most accurate techniques widely used to monitor physical and chemical cross-linking reactions and changes in the material microstructure during the gelation process. This technique investigates the viscoelastic properties during the curing process under small-amplitude oscillatory shear flow without a significant disruption of the microstructure. The viscoelastic behavior of polymer gels near the sol−gel transition has been studied experimentally[22−29] and theoretically.[30−34] Understanding the relationship between gel structure and linear visoelastic behavior at the sol−gel transition was one of the most important goals of these studies.[22−30]

Evaluation and characterization of the gelation process are very crucial to optimize the processing conditions of cross-linked materials. The universal behavior of cross-linked materials at the gel point makes the gelation process interesting from a fundamental point of view.[34−36] Real-time measurements of viscoelastic material parameters (G', G'', and η^*) in the vicinity of the gel temperature are normally used to monitor the formation of gel, where a sudden increase in these parameters can be easily detected at the onset of the gelation process.[27,29] At the gel point a huge increase in the molecular weight of the material is normally expected, where the existence of one long chain running through the whole system with a sudden loss of flow are the most common criteria of gel

dx.doi.org/10.1021/ma301458n | Macromolecules 2012, 45, 7729−7739

Scheme 1. ROMP Process of NCO Using Second-Generation Grubbs Catalyst

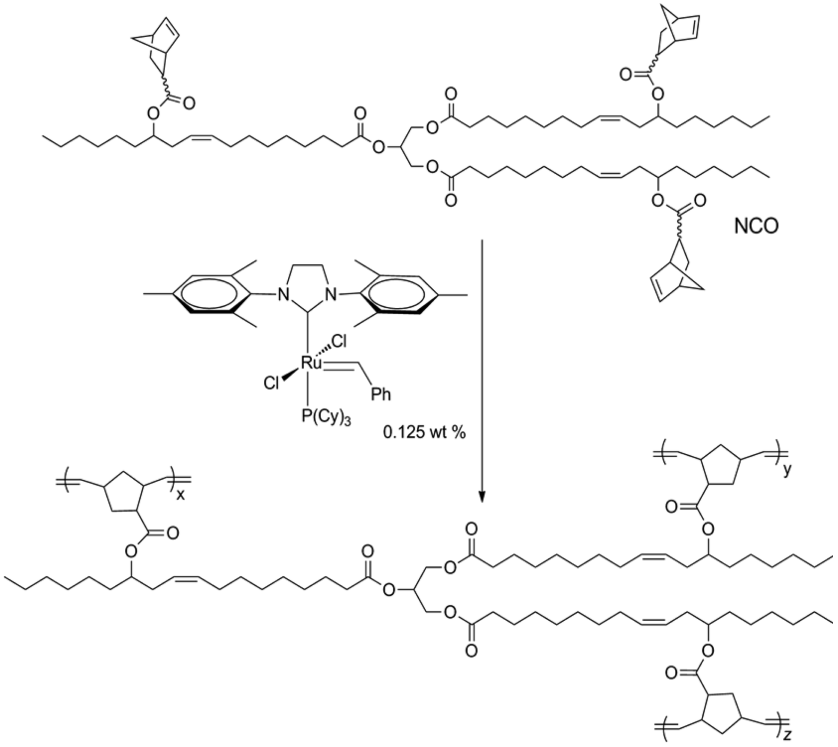

formation.[38−44] Several models for gelation have been proposed, and the most well-known is percolation theory.[45,46] The percolation theory was generalized to predict how the viscoelastic properties are expected to scale with time or frequency.[47] For example, at the gel point, G', G'', and η_0 are expected to follow power law behavior with frequency based on the percolation theory as will be investigated later in this article.

Here, the kinetics of ROMP for norbornenyl-functionalized castor oil (NCO), which has ca. 0.8 norbornene rings per fatty acid chain, are investigated using small-amplitude oscillatory shear flow experiments. The ROMP was carried out using only 0.125 wt % of second-generation Grubbs catalyst to prepare a novel castor oil-based thermoset. The rheokinetics are investigated by evaluating G', G'', η^*, and tan δ during the ROMP process as a function of temperature, angular frequency, and curing time. The real-time evolution measurements of the viscoelastic properties at different constant temperatures and shear frequencies near the T_{gel} are also considered. Furthermore, equilibrium storage modulus, G_{eq}, and zero shear viscosity, η_0, are expressed in power law scaling functions with critical exponents that may be useful in predicting the validity of percolation theory for this bio-based thermoset polymer. The molecular dynamics and thermal stability of the fully cured sample are investigated by dynamic mechanical analysis (DMA) and thermogravimetric analysis (TGA) measurements, respectively.

EXPERIMENTAL SECTION

Materials. Castor oil, second-generation Grubbs catalyst, triethylamine, and acryloyl chloride were obtained from Sigma-Aldrich (Milwaukee, WI), while dicyclopentadiene (DCPD) (purity higher than 95%) was supplied by Alfa Aesar (Ward Hill, MA). Benzene, ethyl acetate, methylene chloride, $NaHCO_3$, and HCl were obtained from Fisher (Fair Lawn, NJ). All reagents were used as received without further purification unless otherwise stated.

Synthesis of Bicyclo[2.2.1]hept-2-ene-5-carbonyl Chloride (BHCC). The detailed description of BHCC synthesis was described elsewhere.[48,49] At 0 °C, 56 g of freshly cracked cyclopentadiene (0.85 mol) was added dropwise to 70 g of acryloyl chloride solution (0.77 mol) in toluene (275 mL). The reaction mixture was kept at 0 °C for 3 h and then heated up to 100 °C and held for 30 min. A yield of 95 g (~79%) as a colorless oil (83:17 endo:exo) was obtained after distillation of toluene and residual liquid under reduced pressure. The ^{1}H NMR of pure BHCC is depicted in Figure 1a. The ^{1}H NMR ($CDCl_3$, δ ppm) of pure BHCC contains both the endo and exo isomers and their peak assignments.

Synthesis of Norbornenyl-Functionalized Castor Oil (NCO). Castor oil (20 g, 0.021 mol) was dissolved in 100 mL of anhydrous CH_2Cl_2 and cooled to 0 °C. A solution of BHCC (10.6 g, 0.068 mol) in 100 mL of anhydrous CH_2Cl_2 was added dropwise, and then 11.4 g of triethylamine (0.11 mol) was added. The solution was heated up to room temperature under constant stirring and maintained at that temperature for 48 h. Subsequently, the reaction mixture was stirred with 500 mL of aqueous 5 wt % Na_2CO_3 solution overnight to convert the excess BHCC into water-soluble carboxylate salt. After extraction with CH_2Cl_2 and removal of the solvent, a quantitative yield of NCO was obtained as a brown liquid. More details about NCO synthesis can be found in our previous publication.[49]

The chemical structure and ^{1}H NMR spectrum of castor oil are shown in Figure 1b. The methylene protons in the glyceride unit are given by the signals at 4.1−4.4 ppm (a), while the vinyl protons (f) in the fatty acid chains are observed at 5.3−5.6 ppm. The tertiary hydrogen atoms adjacent to the hydroxyl group in the fatty acid chain (h) are detected at 3.6 ppm. NCO can be easily synthesized with excellent yield through esterification of castor oil by BHCC. The chemical structure of NCO and its ^{1}H NMR spectrum are also presented in Figure 1b. The peak at 3.6 ppm (h) is substantially reduced in NCO compared to castor oil, indicating that most of the hydroxyl groups have reacted and a new peak representing the tertiary hydrogen adjacent to the norbornenyl ester is observed at 4.8 ppm. Approximately 95% of the hydroxyl groups reacted with BHCC as determined by the integration of the peaks k and h. This calculation suggested that about 2.4 norbornene rings were incorporated into the

dx.doi.org/10.1021/ma301458n | Macromolecules 2012, 45, 7729−7739

triglyceride (0.8 norbornene rings per fatty acid chain). The norbornene hydrogens are found at 5.9−6.2 ppm.

Freeze-Drying of the Grubbs Catalyst. Normally, freeze-drying of the Grubbs catalyst is necessary to improve the solubility of the catalyst in the NCO monomer. Here, the freeze-drying process was carried out according to a literature procedure.[50] About 5 mL of benzene was used to dissolve 250 mg of Grubbs catalyst, and then the solution was quenched in liquid nitrogen. Benzene will be sublimated under vacuum at room temperature for 5 h. The large surface area of the Grubbs catalyst produced from this procedure has excellent solubility in NCO monomer.

Rheological Measurements. Scheme 1 shows the ROMP process of NCO using second-generation Grubbs catalyst. The rheokinetics of the ROMP process was investigated for a mixture of NCO with 0.125 wt % Grubbs catalyst using a TA Instruments (ARES-G2) with 25 mm diameter parallel plates. All rheological measurements (isothermal and nonisothermal) were carried out under very accurate thermal conditions (±0.1 K) using an air/N_2 gas convection oven designed with twin element heater guns, a barrel-shaped chamber, and three internal platinum resistance thermometers (PRT) for optimum temperature stability. In this study, the following rheological experiments were performed:

1. Strain sweep at a constant temperature and angular frequency range of 0.1−100 rad/s to obtain the linear viscoelastic range of the sample.
2. A temperature sweep (2 °C/min) at different constant angular frequencies and a certain strain rate in the linear viscoelastic regime in order to determine the temperature dependence of the linear viscoelastic properties and to evaluate the gelation temperature.
3. A time sweep at different constant temperatures (40, 45, 50, and 55 °C) and constant angular shear frequency (ω = 0.5 rad/s) in the linear viscoelastic regime in order to determine the influence of the ROMP process on the visoelastic characteristic functions (G', G'', and η^*).
4. A frequency sweep at a given constant temperature for different gelation times in the linear viscoelastic region to test the validity of expressing G', G'', and η_0 in power law forms with critical exponents based on the percolation theory.

DSC, DMA, and TGA Measurements. DSC measurement after rheokinetics test at 55 °C for 5 h was investigated to confirm the full curing of the sample. The DSC measurement was conducted using a TA Instruments Q2000. The DSC measurement was carried out in an atmosphere of dry nitrogen. The glass transition temperature (T_g) was determined using the temperature of half the step height in the specific heat curve. The DMA (dynamic mechanical analysis) and TGA (thermogravimetric analysis) measurements for a fully cured sample (5 h at 55 °C, i.e., the time required to reach a complete curing reaction or conversion) were carried out using a Q800 dynamic mechanical analyzer and a Q50 thermogravimetric analyzer (TA Instruments, New Castle, DE), respectively. For DMA measurement, a rectangular shape sample of 0.77 mm thick and 8 mm wide was heated from −90 to 100 at 3 °C/min heating rate at a frequency of 1 Hz. However, for TGA measurement, about 5 mg of the cured sample was heated from 50 to 600 °C under a nitrogen atmosphere at 20 °C/min heating rate.

RESULTS AND DISCUSSION

Effect of Thermal-Induced ROMP on Rheological Behavior. The effect of thermal-induced ROMP for NCO with 0.125 wt % Grubbs catalyst on the viscoelastic properties will be investigated in this section. Figure 2 demonstrates the temperature dependence of G' at a heating rate of 2 °C/min and different constant angular frequencies. At a temperature range lower than the gel temperature ($T \leq 43$ °C), the value of G' slightly decreases with increasing temperature. A sudden increase in G' at about 44 °C (T_{onset}) was observed at all values of angular frequencies owing to the onset formation of a three-dimensional thermoset structure of NCO. The magnitude of

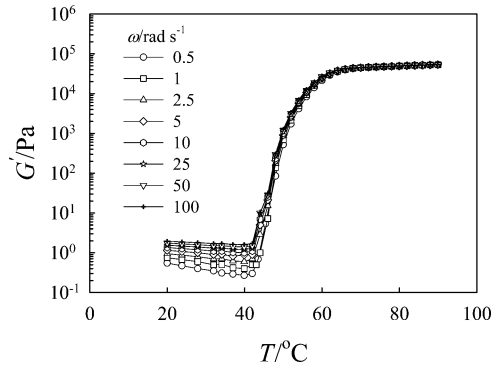

Figure 2. Temperature dependence of dynamic storage modulus, G', for the ROMP process of NCO at 2 °C/min heating rate and different constant angular frequencies.

the elevation in G' increases greatly with increasing temperature because of the evolution of the ROMP process and the significant increase in branching (formation of cross-linked structure). In addition, G' is no longer frequency dependent at a high temperature range because of the formation of an equilibrium storage modulus, G_{eq}, which is a typical criterion for the formation of a cross-linked structure.

The complex shear viscosity η^* behaves differently with angular frequency and temperature, as shown in Figure 3. At

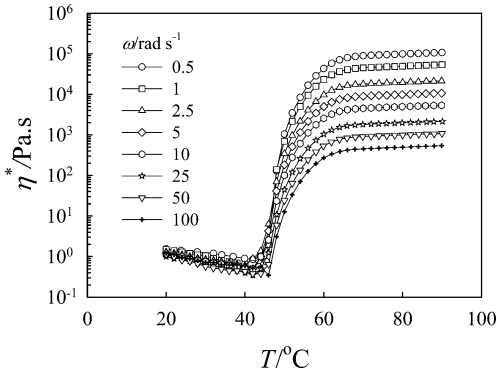

Figure 3. Temperature dependence of complex viscosity, η^*, for the ROMP process of NCO at 2 °C/min heating rate and different constant angular frequencies.

low temperatures, η^* is almost constant, regardless of angular frequency, and slightly decreases with increasing temperature. At higher temperatures, η^* becomes strongly frequency dependent (non-Newtonian behavior). This different behavior of η^* is attributed to the fact that, at low temperatures (i.e., $T <$ 46 °C), the NCO was not totally polymerized and exhibited almost frequency-independent viscosity behavior over the entire range of angular frequencies (Newtonian behavior). At T_{onset}, the NCO changed from a liquid-like to a solid-like structure, and consequently η^* becomes frequency dependent as the ROMP process evolves into the formation of a cross-linked polymer structure. Therefore, the different behavior of η^* with temperature and frequency is not surprising. Details of the frequency dependence of η^* over a wide range of temperatures and angular frequencies will be considered in the next section.

The kinetics of thermal-induced ROMP of NCO can be investigated rheologically by monitoring the variation of viscoelastic material parameters, such as G', G'', η^*, and η_0, at

dx.doi.org/10.1021/ma301458n | Macromolecules 2012, 45, 7729−7739

different constant temperatures, curing times, and angular frequencies. Here, it is imperative to accurately determine T_{gel}, which is the temperature at which the three-dimensional cross-linked structure of thermoset NCO is formed. The T_{gel} will be evaluated by two different methods. With the first method, T_{gel} will be determined from the simultaneous temperature dependence of the dynamic shear moduli, G' and G'', as shown in Figure 4. At temperatures below T_{onset}, both G' and

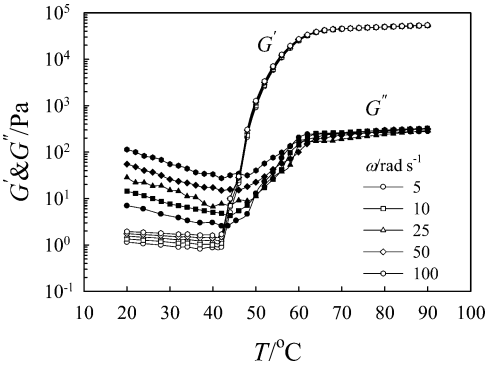

Figure 4. Temperature dependence of G' and G'' for the ROMP process of NCO at 2 °C/min heating rate and different constant angular frequencies.

G'' are frequency dependent and G'' is more than 1 order of magnitude higher than G'. As the temperature increases and T_{onset} is approached, both G' and G'' increase with temperature and coincide at T_{gel}. At higher temperatures than T_{gel}, the ROMP process evolves and G' increases more rapidly than G'' (i.e., G' is ~2 orders of magnitude higher than G''), indicating the formation of a three-dimensional cross-linked polymer structure. It is also clear that the evaluation of T_{gel} from the crossover of G' and G'' is slightly angular frequency dependent (T_{gel} is approximately 44 and 47 °C at ω = 5 and 100 rad/s, respectively). However, it is well established in the literature that the crossover of G' and G'' is not a general criterion for the determination of T_{gel} because of its high frequency dependence.[51,52] In a previous work, we have reported that the T_{gel} of thermally cross-linked poly(vinyl methyl ether) evaluated at ω = 100 rad/s was ca. 20 °C higher than that obtained at ω = 1 rad/s.[51] A similar behavior was reported by Zhao et al.,[52] who found that the temperature at which G' and G'' intersect was shear stress and frequency dependent for sol−gel transition of a hybrid gel. Winter et al.[22,23] reported that, when the gelation point cannot be evaluated from the crossover of G' and G'', it could be related to the critical conversion point of the cross-linking reaction. On the basis of the above discussion, it can be concluded that at T_{gel} the polymer chain branching becomes significant and the polymer network starts to form. For $T > T_{gel}$ the branching proceeds, ultimately leading to the formation of a three-dimensional polymer structure characterized by $G' > G''$. In addition, both G' and G'' reach equilibrium values (or become frequency independent). The preceding discussion indicates the rheological material parameters (G', G'', and η^*) of NCO are very sensitive to the thermal-induced ROMP process and the corresponding formation of a cross-linked polymer structure.

An alternative method to evaluate T_{gel} relies on the temperature dependence of the zero-shear viscosity, η_0. The magnitude of η_0 will increase dramatically once T_{gel} is reached. The angular frequency dependence of η^* must be carried out over a wide range of temperatures below and above T_{gel} (44 °C) for NCO to evaluate η_0 as a function of temperature. A typical angular frequency dependence of η^* at different constant temperatures is shown in Figure 5.

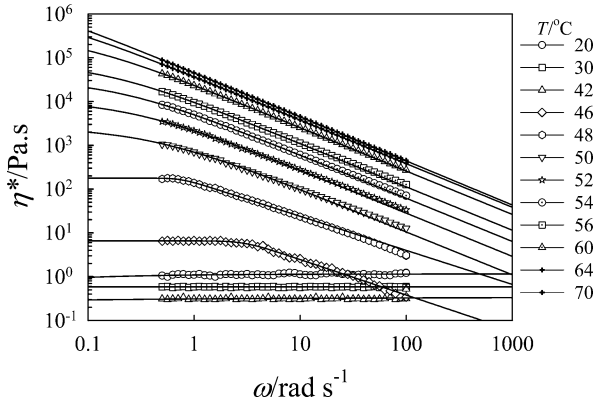

Figure 5. Angular frequency dependence of complex viscosity, η^*, for the ROMP process of NCO at different constant temperatures. The lines are calculated from eq 1, while the symbols represent experimental data.

Obviously, the viscosity decreases gradually with increasing temperature at temperatures lower than the T_{gel} (i.e., $T \leq 42$ °C) while it exhibits Newtonian behavior (frequency independent). At higher temperatures ($T \geq 46$ °C), the viscosity increases strongly with increasing temperature; for example, at 70 °C the viscosity is ~6 orders of magnitude higher than the corresponding value at 42 °C. In this temperature range, the viscosity decreases strongly with increasing angular frequency (non-Newtonian behavior). The value of η_0 at different temperatures can be accurately determined by fitting the η^* versus ω curves according to the Carreau−Yasuda model[53]

$$|\eta^*| = \eta_0[1 + (\tau_\eta\omega)^a]^{(n-1)/a} \quad (1)$$

where n and a are material constants, while τ_η is a characteristic viscous relaxation time that defines the location of the transition from Newtonian to shear-thinning behavior. Using the Carreau−Yasuda model resulted in an excellent description of the experimental data, as shown in Figure 5, where the lines are fitting lines and the symbols are the experimental data. Table 1 shows the characteristic rheological parameters for the NCO at different curing temperatures during the rheokinetics reaction using eq 1.

Figure 6 depicts the temperature dependence of η_0 obtained from fitting the data in Figure 5 to eq 1. Figures 5 and 6 clearly show that η_0 follows the same trend as the dynamic temperature ramps of G', G'', and η^* (Figures 2−4), with a sudden increase in the value of η_0 at T_{gel}. T_{gel} can be determined by the intersection of the tangent lines to the experimental data as shown in Figure 6 where the arrow indicates the value of the T_{gel}, determined by this method. The T_{gel} obtained using this method (44 °C) is identical to the value determined using the crossover point of G' and G'' at ω = 0.5 rad/s (see Figure 4).

Real-Time Rheological Measurements during ROMP. In this section, the time evolution of the viscoelastic properties during the ROMP process of NCO in the vicinity of T_{gel} is investigated. Figure 7 shows the isothermal time dependence of G' at different constant temperatures and an angular frequency

dx.doi.org/10.1021/ma301458n | Macromolecules 2012, 45, 7729−7739

Table 1. Characteristic Rheological Parameters for the NCO at Different Curing Temperatures during the Rheokinetics Reaction Using Eq 1

T/°C	η_0/Pa·s	τ_η/s	n	a
20	1.15	1.8×10^{-5}	0.35	0.51
30	0.58	3.1×10^{-5}	0.37	0.49
42	0.37	5.8×10^{-6}	0.51	0.53
46	7	5.7×10^{-3}	0.18	0.39
48	287	0.033	0.41	0.33
50	2541	0.07	0.38	0.51
52	1.07×10^4	1.32	0.25	0.34
54	3.22×10^4	1.8	0.31	0.44
56	8.06×10^4	2.7	0.19	0.37
60	3.61×10^5	3.1	0.21	0.41
64	1.35×10^6	3.3	0.34	0.51
70	3.06×10^6	3.5	0.23	0.53

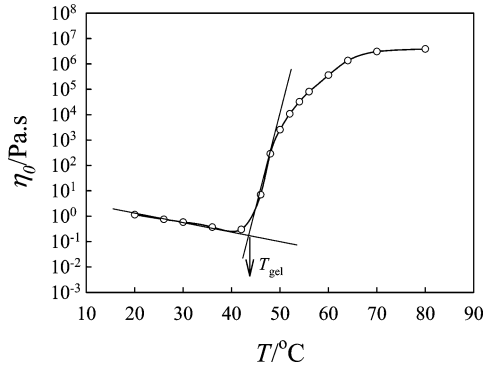

Figure 6. Zero-shear viscosity as a function of temperature for the ROMP process of NCO. The arrow shows the value of T_{gel}.

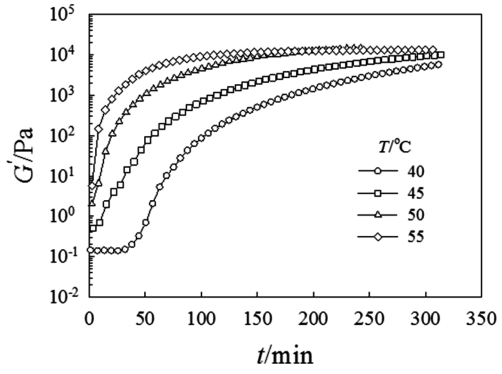

Figure 7. Time dependence of G' at different constant temperatures and ω = 0.5 rad/s for the ROMP process of NCO.

of ω = 0.5 rad/s. Obviously, a dramatic increase in G' was observed at the early and intermediate stages of the ROMP process (t < 100 min) at all measuring temperatures, caused by the formation of a cross-linked network structure. The increase in G' levels off at longer times (i.e., G' becomes almost time independent). The magnitudes of the increase in G' and the time at which G' levels off (t_{lo}) were found to be strongly temperature-dependent; i.e., the magnitude of the elevation in G' increases and t_{lo} decreases with increasing temperature. The fact that the magnitude of the elevation in G' increases greatly with increasing time and temperature is attributed to the gelation process and the significant increase in branching (formation of cross-linked structure). The plateau value of G' at longer times is curing temperature dependent and related to an equilibrium modulus, G_{eq} (a typical criterion for the formation of a cross-linked structure). At 55 °C the ROMP process is significantly faster, implying that the curing time needed to reach the plateau region is shorter than the one observed at lower temperatures. Similar behavior was observed for the curing time dependence of η^* at different curing temperatures and ω = 0.5 rad/s, as shown in Figure 8. Similar behavior was

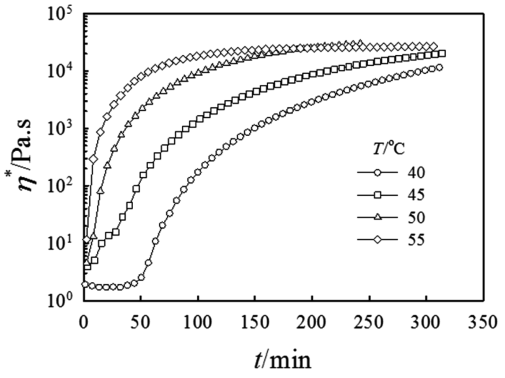

Figure 8. Time dependence of η^* at different constant temperatures and ω = 0.5 rad/s for the ROMP process of NCO.

also found for G'' versus curing time. The elevation of G'' with increasing curing time was found to be relatively small compared to that of G' at a constant temperature under the same rheological conditions (angular frequency and strain rate). This experimental finding is attributed to the elastic origin of the stress induced in the system by the formation of three-dimensional thermoset polymer via ROMP as will be discussed in the next section.

The thermal-induced ROMP of NCO is also examined as a function of different angular frequencies under isothermal conditions. Figure 9 shows the time dependence of G' at 50 °C

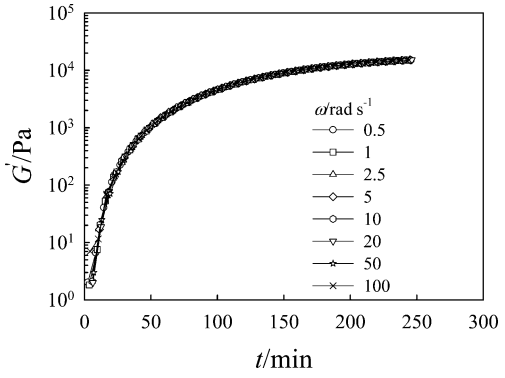

Figure 9. Variation of G' as a function of time for the ROMP process of NCO at 50 °C and different constant angular frequencies.

for different constant angular frequencies. Clearly, the variation of G' with time and frequency can be divided into two different regimes. At t < 150 min (regime I), G' increases rapidly with curing time. In this regime, the chain branching of NCO becomes significant and the formation of a cross-linked structure starts. At t > 150 min (regime II), G' is slightly time dependent as the ROMP process is almost completed. It is also obvious that G' is frequency independent in both regimes I

dx.doi.org/10.1021/ma301458n | Macromolecules 2012, 45, 7729–7739

and II because of the formation of an equilibrium modulus, G_{eq}, which in turn is related to the fast ROMP process at 50 °C.

Figure 10 shows η^* as a function of curing time at 50 °C for different angular frequencies. Here, η^* exhibits almost a

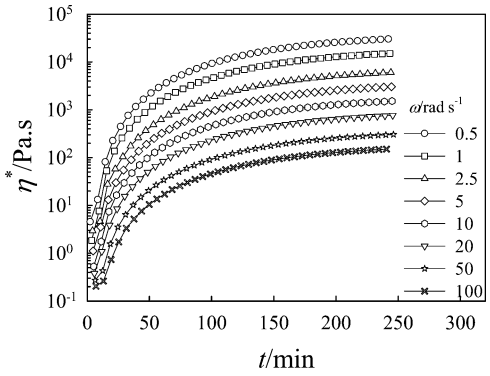

Figure 10. Variation of η^* as a function of time for the ROMP process of NCO at 50 °C and different constant angular frequencies.

Newtonian behavior (frequency independent) at the beginning of the measurement (early stage of the curing process). With increasing time, η^* increases dramatically, reaching equilibrium values that are strongly frequency dependent (non-Newtonian behavior).

Determination of t_{gel}. The Winter–Chambon criterion is the most widely used method to accurately determine gelation time, t_{gel}, of physically and chemically cross-linked materials from their rheological data.[22,23] Based on this criterion, t_{gel} is identified as the instant in time when the dynamic shear moduli, G' and G'', scale in an identical fashion with time; i.e., both can be described by the following power law:

$$G' \sim G'' \sim w^n \tag{2}$$

The relaxation exponent, n, is linked to the microstructural parameters of the cross-linked material. If G' and G'' behave according to the above power law over a sufficiently wide range of angular frequencies, the loss tangent, tan δ, can be expressed by the following equation:

$$\tan\delta = \frac{G''}{G'} = \tan\left(\frac{n\pi}{2}\right) \tag{3}$$

According to eq 3, tan δ is angular frequency independent at t_{gel}. This theory is valid for a variety of physically and chemically cross-linking systems. The time dependence of tan δ for the ROMP process of NCO at 40 °C and different constant angular frequencies is presented in Figure 11. Clearly, tan δ is angular frequency independent at t_{gel} = 70 min, indicating that the cluster structure is macroscopically percolated. At a longer time, tan δ decreases gradually because the increase in G' is higher than the increase in G'' as a result of the formation of a cross-linked polymer structure. It is also clear that before reaching t_{gel} the value of tan δ decreases with increasing ω, however, after t_{gel} the trend reverses. This common behavior has been observed for many systems during physical and chemical gelation reactions and is related to the magnitudes of G' and G'' before and after t_{gel} at different angular frequencies. These results suggest that the Winter–Chambon theory is applicable to this system over a wide range of angular frequencies (as shown in Figure 11), suggesting the existence of a self-similar structure (or critical gel) at the gel point.

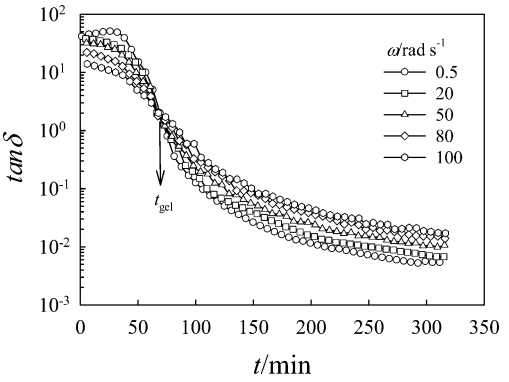

Figure 11. Loss tangent, tan δ, as a function of time at 40 °C for the ROMP process of NCO at different constant shear frequencies. The gel point, t_{gel}, is determined by the intersection point as described by the arrow.

Figure 12 shows the time dependence of G' and G'' at 40 °C and ω = 0.5 rad/s. Clearly, G' is about 2 orders of magnitude

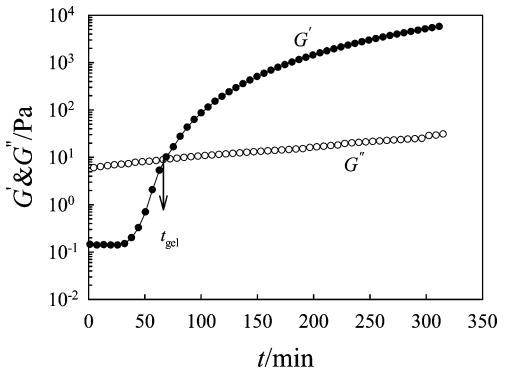

Figure 12. Time dependence of G' and G'' at 40 °C and 0.5 rad/s. The arrow shows t_{gel} as obtained from the crossover point of G' and G''.

lower than G'' at the beginning of the measurement, indicating that the sample exhibits liquid-like behavior. While both G' and G'' increase with time, G' increases more sharply than G'' and becomes about 3 orders of magnitude greater than G'' at the late stage of the curing process (t = 300 min). G' increases at a more rapid rate than G'' because at long curing times above the gel point the elastic effects dominate, owing to the fact that cross-linked structures are capable of storing elastic energy. The gel time t_{gel} can be calculated from the crossover point of G' and G'', as indicated by the arrow in Figure 12. The value of t_{gel} = 70 min obtained from this method is identical to that obtained using tan δ versus t at different frequencies (Figure 11).

Critical Phenomena at Gel Point. The angular frequency dependence of G' at different curing time intervals for the ROMP process of NCO at 40 °C is shown in Figure 13. The figure shows that the slope of G' versus ω decreases dramatically and the magnitude of G' increases greatly with increasing curing time. In addition, G' becomes no longer frequency dependent and reaches an equilibrium value (G_{eq}) at the late stage of the curing process owing to the formation of an elastic, cross-linked structure. Figure 14 shows the angular frequency dependence of G'' for different curing times. In contrast to the behavior of G' with respect to angular frequency, G'' is more angular frequency dependent and does

dx.doi.org/10.1021/ma301458n | Macromolecules 2012, 45, 7729–7739

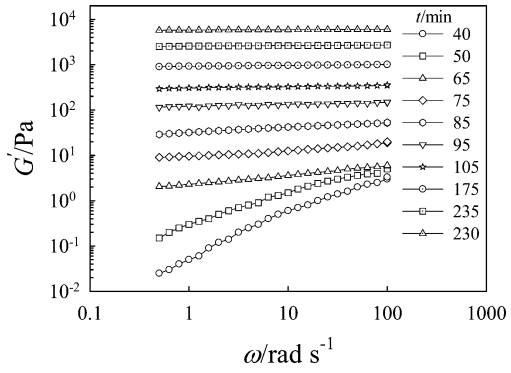

Figure 13. Angular frequency dependence of G' for the ROMP process of NCO at 40 °C for different curing times.

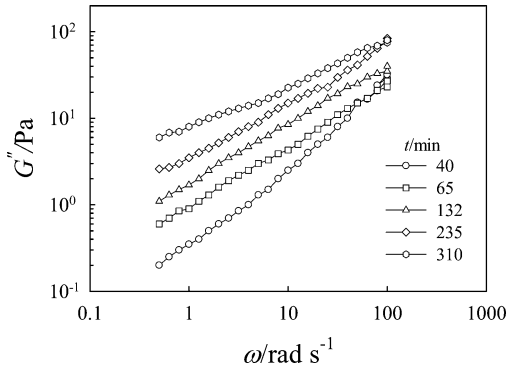

Figure 14. Variation of G'' as a function of angular frequency for the ROMP process of NCO at 40 °C for different curing times.

not dramatically increase with increasing curing time as shown in Figure 14. The smaller increase of G'' with curing time compared to G' under the same conditions (same curing time and temperature) is attributed to the higher sensitivity of G' to the structure change accompanying the cross-linking process. This higher sensitivity of G' to the cross-linking process is attributed to the fact that the stress induced in the system by the branching and formation of a three-dimensional polymer network is mostly of elastic origin. In addition, G'' does not reach a plateau value. The variation of η^* as a function of angular frequency for different curing times at 40 °C is shown in Figure 15. Observably, η^* is slightly frequency dependent at t = 40 min (before the onset of the gelation process). At longer curing times, the value of η^* increases abruptly and the entire curve becomes strongly frequency dependent. In this figure the

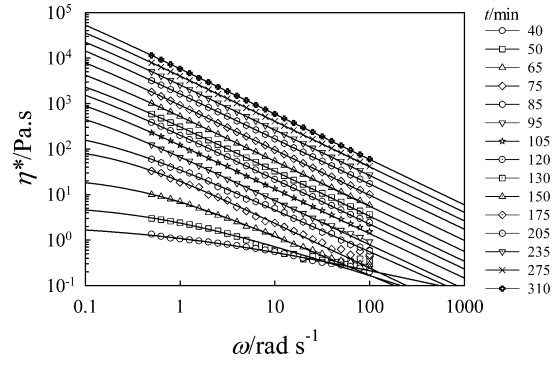

Figure 15. Angular frequency dependence of η^* for the ROMP process of NCO at 40 °C for different curing times.

solid lines are computed from eq 1, while the points represent experimental data.

Analysis of the data in Figures 13 and 14 shows that the variations of G' and G'' with angular frequency follow the power law of eq 2 over the entire range of frequencies. The values of the exponents n' and n'' at different curing times can be obtained from the slopes of G' and G'' versus ω, respectively. One can see that both n' and n'' are curing time dependent, and Figure 16 displays their time dependence at 40

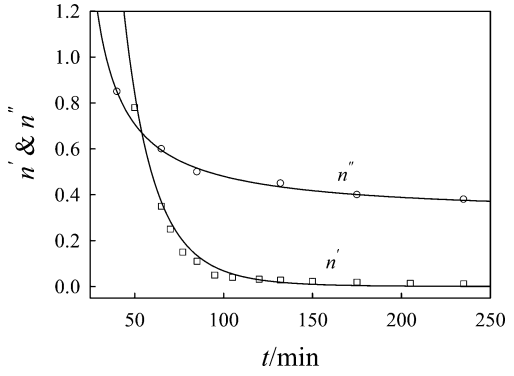

Figure 16. Variation of exponents n' and n'' as a function of time obtained from the slopes of G' and G'' versus ω at 40 °C, respectively, according to eq 2.

°C for the ROMP process of NCO. The values of the two exponents decrease exponentially with curing time and become identical at the gel point; i.e., at t_{gel}, $n = n' = n'' = 0.64$. The values of the exponents are very close to those obtained for different systems reported in the literature and found to be in good agreement with the one predicted theoretically from the percolation theory ($n = 2/3$).[54−58]

In the vicinity of the gel point, both η_0 and G_{eq} also can be expressed as power law scaling functions based on the following equations:

$$\eta_0 \sim \varepsilon^{-k} \quad (P < P_c) \tag{4}$$

$$G_{eq} \sim \varepsilon^{z} \quad (P > P_c) \tag{5}$$

where P and P_c are the reaction extents at time t and t_{gel}, respectively, while ε is the relative distance from the gel point, which can be determined by eq 6:

$$\varepsilon = \frac{|P - P_c|}{P_c} \tag{6}$$

The values of G_{eq} at different curing times can be determined by the frequency-independent values of G' in Figure 13 (G' is almost frequency independent at $t_{gel} \geq 65$ min). The corresponding values of η_0 can be determined by fitting the angular frequency dependence of η^* to eq 1, as demonstrated in Figure 15.

Figure 17 depicts G_{eq} and η_0 as a function of ε in a double-logarithmic scale; the slopes of the two linear curves directly determine the values of z and k, respectively. From the critical exponents k and z, one can calculate the exponent n from the following equation:[59]

$$n = \frac{z}{k + z} \tag{7}$$

dx.doi.org/10.1021/ma301458n | Macromolecules 2012, 45, 7729−7739

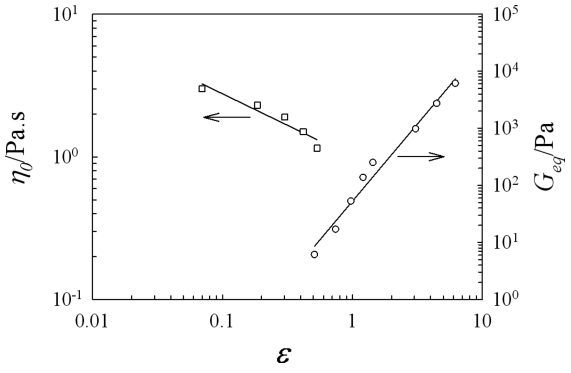

Figure 17. Dependence of η_0 and G_{eq} on the relative distance from the gel point, ε, in a double-logarithmic scale at 40 °C.

The values of z and k obtained from the slopes of the two curves of Figure 17 are 2.1 and 0.75, respectively, yielding a value of $n = 0.73$. This value is in acceptable agreement with the value obtained from Figure 16. On the basis of the discussion in the preceding sections, it is apparent that the ROMP process of bio-based NCO thermosets can be well characterized by its viscoelastic properties during the curing process. In addition, the critical phenomenon near the gel point can be well described by the scaling power laws based on percolation theory and Winter−Chambion approaches.

DSC, DMA, and TGA Measurements. The DSC measurement for the sample that was isothermally cured at 55 °C and 0.5 rad/s for 5 h during the rheokinetics study (see Figure 7) was carried out to detect any addition isothermal curing process in the sample. The DSC data (Figure 18a) showed only one T_g for NCO at −50 °C without any isothermal curing process, indicating that the sample was fully cured during the rheokinetics measurement under the just mentioned curing condition.

The DMA measurement for a fully cured sample under identical condition to that used to cure the sample in the rheometer (5 h at 55 °C) is shown in Figure 18b, which demonstrates the temperature dependence of the storage modulus (E') and tan δ at 1 Hz and 3 °C/min heating rate. Only one glass relaxation process (α-relaxation) was observed at approximately −17 °C (the peak maxima of tan δ). This peak is related to the micro-Brownian cooperative reorientation of the polymeric chains and is related to the T_g of the material. This relaxation process is frequency dependent and normally appears above the calorimetric T_g of the material. At a low temperature range ($T \leq -40$ °C), E' is constant regardless of the increase in temperature. A dramatic decrease in E' was observed at the same temperature range corresponding to that of the tan δ peak. The value of E' becomes temperature independent and reaches a plateau at higher temperatures due to the cross-linked structure of the polymer network in the rubbery region. The cross-link density (ν_e) of this materials can be evaluate from the plateau value of E' at 50 °C above the T_g of the material based on the kinetic theory of rubber elasticity (i.e., $E' = 3\nu_e RT$).[60,61] The cured sample was found to have a cross-link density of $\nu_e = 318$ mol/m.[3]

The thermal stability of the fully cured sample was investigated using thermogravimetry. Figure 19 shows a typical TGA measurement for this sample at 20 °C/min heating rate under a nitrogen atmosphere. One can see that the sample is thermally stable at temperatures up to 200 °C. About 10 wt % of the sample is degraded at approximately 200−300 °C. This

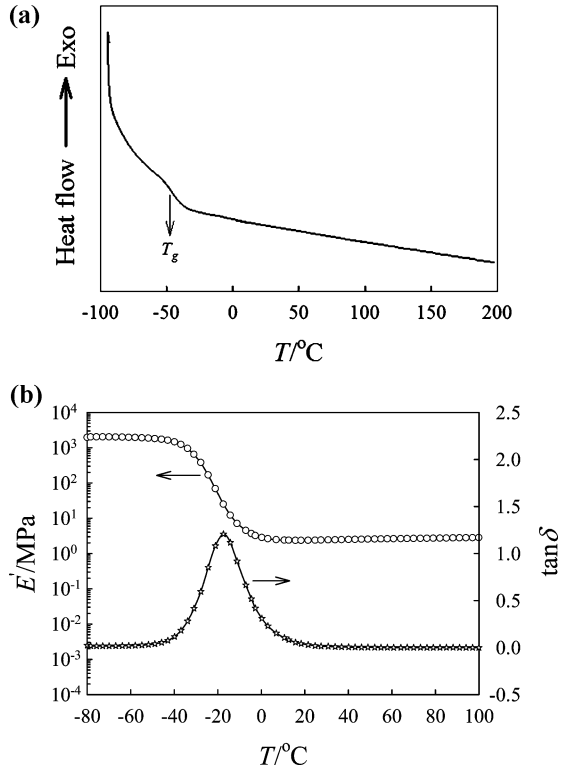

Figure 18. (a) DSC thermogram for fully cured sample after rheokinetics measurement at 55 °C for 5 h and 0.5 rad/s angular frequency. The arrow shows the T_g of the cured sample. (b) Dynamic storage modulus, E', and tan δ as a function of temperature for fully cured NCO sample at 3 °C/min heating rate and 1 Hz.

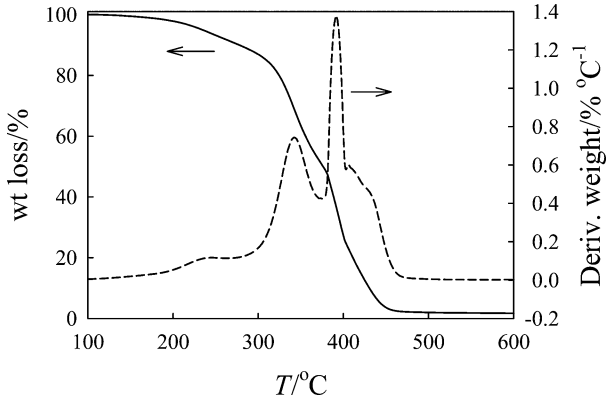

Figure 19. TGA measurement for fully cured NCO sample at 20 °C/min heating rate under a nitrogen atmosphere.

process is related to the evaporation of soluble materials and unreacted oil fragments. With increasing temperature up to 500 °C, two fast degradation processes were observed. In the first one in the temperature range 300−370 °C, about 50 wt % of the sample was lost due to the degradation of the polymer backbone. The second process at around 380−500 °C is believed to be caused by further decomposition of the cross-linked fragments. The different thermal degradation processes of the fully cured NCO can be easily observed in the TGA derivative curve as shown in the dashed line of Figure 19. The multiple thermal degradation processes of bio-based thermoset polymers from vegetable oils are discussed elsewhere in the literature.[62,63]

dx.doi.org/10.1021/ma301458n | Macromolecules 2012, 45, 7729−7739

CONCLUSION

The thermal-induced curing of norbornenyl-functionalized castor oil with a controlled amount of 0.8 norbornene rings per fatty acid chain via ROMP was investigated rheologically under different curing time, temperature, and angular frequency conditions.

A dramatic increase in the viscoelastic material functions (G', G'', and η^*) at the onset of the ROMP process was observed during the dynamic temperature ramp experiments. The temperature dependence of zero-shear viscosity, η_0, was found to follow the same trend as the one observed in the temperature ramps of G' and G'' (i.e., a dramatic increase in η_0 is observed at T_{gel}). The T_{gel} determined by the crossover point of G' and G'' was in good agreement with the value obtained from the temperature dependence of η_0. The real-time evolution of the ROMP process of NCO was also investigated by measuring G', G'', η^*, and tan δ at constant different temperatures (40, 45, 50, and 55 °C) and angular frequencies. The value of t_{gel} determined by the time dependence of tan δ (the point at which all curves of tan δ coincide and are angular frequency independent) was found to be applicable over a wide range of angular frequencies according to the Winter–Chambon method and identical to the value obtained from the crossover point of G' and G''. Furthermore, both G' and G'' were found to follow a power law behavior as a function of angular frequency ($G' \sim G'' \sim \omega^n$) with exponents n' and n'' that are strongly dependent on curing time in good agreement with that predicted theoretically based on the percolation theory. Both η_0 and G_{eq} were also expressed in power law scaling functions with the relative distance from the gel point, $\eta_0 \sim \varepsilon^{-k}$ and $G_{eq} \sim \varepsilon^z$ with $k = 0.75$ and $z = 2.1$. The value of the exponent n obtained from the slopes k and z is 0.73, in close agreement with the value predicted theoretically from the percolation theory ($n = 2/3$). The cured sample was thermally stable up to 200 °C and showed only one α-relaxation process as confirmed by TGA and DMA measurements, respectively.

AUTHOR INFORMATION

Corresponding Author

*Tel 515-294-3101; e-mail mkessler@iastate.edu.

Notes

The authors declare no competing financial interest.

REFERENCES

(1) Ogunniyi, D. S. *Bioresour. Technol.* **2006**, *97*, 1086–1091.
(2) Sharma, V.; Kundu, P. P. *Prog. Polym. Sci.* **2008**, *33*, 1199–215.
(3) Trnka, T. M.; Grubbs, R. H. *Acc. Chem. Res.* **2001**, *34*, 18–29.
(4) Meier, M. A. R. *Macromol. Chem. Phys.* **2009**, *210*, 1073–1079.
(5) Henna, P. H.; Larock, R. C. *Macromol. Mater. Eng.* **2007**, *292*, 1201–1209.
(6) Kodali, D. R. U.S. Patent 6420322, 2002.
(7) Henna, P.; Larock, R. C. *J. Appl. Polym. Sci.* **2009**, *112*, 1788–1797.
(8) Matsumoto, A.; Miwa, Y.; Inoue, S.; Enomoto, T.; Aota, H. *Macromolecules* **2010**, *43*, 6834–6842.
(9) Scariah, K. J.; Usha, K. M.; Narayanaswamy, K.; Shanmugam, K.; Sastri, K. S. *J. Appl. Polym. Sci.* **2003**, *90*, 2517–2524.
(10) Krishnan, P.; Gopala, S.; Chaobin, H. *Macroml. Chem. Phys.* **2003**, *204*, 531–539.
(11) Hwang, S.-H.; Lee, G.-S. *Eur. Polym. J.* **2000**, *36*, 2305–2308.
(12) Wright, M. E.; Schorzman, D. A.; Pence, L. E. *Macromolecules* **2000**, *33*, 8611–8617.
(13) Mititelu, A.; Hamaide, T.; Novat, C.; Dupuy, J.; Cascaval, C. N.; Cristofor, B.; Patrick Navard, S. *Macroml. Chem. Phys.* **2000**, *201*, 1209–1213.
(14) Urbaczewski, E.; Pascault, J. P.; Sautereau, H.; Riccardi, C. C.; Moschiar, S. S.; Williams, R. J. *Makromol. Chem.* **1990**, *191*, 943–953.
(15) Montserrat, S.; Martin, J. G. *J. Appl. Polym. Sci.* **2002**, *85*, 1263–1276.
(16) Ivankovic, M.; Dzodan, N.; Brnardic, I.; Mencer, H. J. *J. Appl. Polym. Sci.* **2002**, *83*, 2689–2698.
(17) Leroy, E.; Dupuy, J.; Maazouz, A. *Macromol. Chem. Phys.* **2001**, *202*, 465–474.
(18) Flammersheim, H.-J.; Opfermann, J. R. *Macromol. Mater. Eng.* **2001**, *286*, 143–150.
(19) Ton-That, M.-T.; Cole, K. C.; Jen, C.-K.; Franca, D. R. *Polym. Compos.* **2000**, *21*, 605–618.
(20) Hopewell, J. L.; George, G. A.; Hill, D. J. T. *Polymer* **2000**, *41*, 8231–8239.
(21) Brill, R. P.; Palmese, G. R. *J. Appl. Polym. Sci.* **2000**, *76*, 1572–1582.
(22) Chambon, F.; Winter, H. H. *J. Rheol.* **1987**, *31*, 683–697.
(23) Winter, H. H.; Morganelli, P.; Chambon, F. *Macromolecules* **1988**, *21*, 532–535.
(24) Scanlan, J. C.; Winter, H. H. *Macromolecules* **1991**, *24*, 47–54.
(25) Zhu, J.; Wei, S.; Ryu, J.; Budhathoki, M.; Liang, G.; Guo, Z. *J. Mater. Chem.* **2010**, *20*, 4937–4948.
(26) Adolf, D.; Martin, J. E.; Wilcoxon, J. P. *Macromolecules* **1990**, *23*, 527–531.
(27) Madbouly, S. A.; Otaigbe, J. U.; Nanda, A. K.; Wicks, D. A. *Macromolecules* **2005**, *38*, 4014–4023.
(28) Madbouly, S. A.; Otaigbe, J. U. *Macromolecules* **2006**, *39*, 4144–4151.
(29) Madbouly, S. A.; Otaigbe, J. U. *Prog. Polym. Sci.* **2009**, *34*, 1283–1332.
(30) Takahashi, M.; Yokoyama, K.; Masuda, T.; Takigawa, T. J. *Chem. Phys.* **1994**, *101*, 798–804.
(31) Muthukumar, M. J. *Chem. Phys.* **1985**, *83*, 3162–3168.
(32) Takigawa, T.; Takahashi, M.; Urayama, K.; Masuda, T. *Chem. Phys. Lett.* **1992**, *195*, 509–512.
(33) Hess, W.; Vilgis, T. A.; Winter, H. H. *Macromolecules* **1988**, *21*, 2536–2542.
(34) Muthukumar, M. *Macromolecules* **1989**, *22*, 4656–4658.
(35) Lairez, D.; Adam, M.; Emery, J. R.; Durand, D. *Macromolecules* **1992**, *25*, 286–289.
(36) Adolf, D.; Martin, J. R.E. *Macromolecules* **1991**, *24*, 6721–6724.
(37) Zhao, Y.; Cao, Y.; Yang, Y.; Wu, C. *Macromolecules* **2003**, *36*, 855–859.
(38) Grisel, M.; Muller, G. *Macromolecules* **1998**, *31*, 4277–4281.
(39) Hone, J. H. E.; Howe, A. M.; Cosgrove, T. A. *Macromolecules* **2000**, *33*, 1199–1205.
(40) Balan, C.; Völger, K. W.; Kroke, E.; Riedel, R. *Macromolecules* **2000**, *33*, 3404–3408.
(41) Daoud, M. *Macromolecules* **2000**, *33*, 3019–3022.
(42) Yoon, P. J.; Han, C. D. *Macromolecules* **2000**, *33*, 2171–2183.
(43) Tanaka, F. *Macromolecules* **1998**, *31*, 384–393.
(44) Matricardi, P.; Dentini, M.; Crescenzi, V. *Macromolecules* **1993**, *26*, 4386–4387.
(45) Stauffer, D. *Introduction to Percolation Theory*; Taylor and Francis: London, 1985.
(46) De Gennes, P.-J. *Scaling Concepts in Polymer Physics*; Cornell University Press: Ithaca, NY, 1979.
(47) Schiessel, H.; Blument, A. *Macromolecules* **1995**, *28*, 4013–4019.
(48) Arehart, S. V.; Pugh, C. *J. Am. Chem. Soc.* **1997**, *119*, 3027–337.
(49) Xia, Y.; Larock, R. C. *Polymer* **2010**, *51*, 2508–2514.
(50) Jones, A. S.; Rule, J. D.; Moore, J. S.; White, S. R.; Sottos, N. R. *Chem. Mater.* **2006**, *18*, 1312–1317.
(51) Madbouly, S. A.; Ougizawa, T. *J. Macromol. Sci., Phys.* **2004**, *B43*, 655–670.
(52) Zhao, Y.; Cao, Y.; Yang, Y.; Wu, C. *Macromolecules* **2003**, *36*, 855–859.

(53) Carreau, P. J.; De Kee, D.; Chhabra, R. P. *Rheology of Polymeric Systems: Principles and Applications*; Hanser: Munich, 1997.
(54) Takenaka, M.; Kobayashi, T.; Hashimoto, T.; Takahashi, M. *Phys. Rev. E* **2002**, *65*, 041401−041407.
(55) Takenaka, M.; Kobayashi, T.; Saijo, K.; Tanaka, H.; Iwase, N.; Hashimoto, T.; Takahashi, M. *J. Chem. Phys.* **2004**, *121*, 3323−3328.
(56) Groot, R. D.; Agterof, W. G. M. *Macromolecules* **1995**, *28*, 6284−6295.
(57) Kioniksen, A.-L.; Nystrom, B. *Macromolecules* **1996**, *29*, 5215−5222.
(58) Choi, J. H.; Ko, S.-W.; Kim, B. C.; Blackwell, J.; Lyoo, W. S. *Macromolecules* **2001**, *34*, 2964−2972.
(59) Martin, J. E.; Adolf, D.; Wilcoxon, J. P. *Phys. Rev. A* **1989**, *39*, 1325−1332.
(60) Flory, P. J. *Principles of Polymer Chemistry*; Cornell Univerisity Press: Ithaca, NY, 1953.
(61) Ward, I. M. *Mechanical Properties of Solid Polymers*; Wiley-Interscience: New York, 1971.
(62) Xia, Y.; Lu, Y.; Larock, R. C. *Polymer* **2010**, *51*, 53−61.
(63) Andjelkovic, D. D.; Valverde, M.; Henna, P.; Li, F.; Larock, R. C. *Polymer* **2005**, *46*, 9674−9685.